JTTEE5 16:96–103
DOI: 10.1007/s11666-006-9011-6
1059-9630/$19.00 © ASM International

Peer Reviewed

# Plasma-Sprayed Beryllium on Macro-Roughened Substrates for Fusion Reactor High Heat Flux Applications

*Kendall J. Hollis, Brian D. Bartram, Manfred Roedig, Dennis Youchison, and Richard Nygren*

*(Submitted September 21, 2006; in revised form November 20, 2006)*

**The development of beryllium first wall (FW) plasma facing components for future magnetic confinement fusion experiments, such as the International Thermonuclear Experimental Reactor (ITER), is a topic of great importance as research into long-term energy sources increases in urgency. The FW components must be able to survive the harsh plasma environment for extended periods of time. One proposed method for initial fabrication and repair of FW components is plasma spraying. Previous plasma-sprayed beryllium mock-up FW components had coating separation from the substrate at the edges. The present work describes experiments to produce beryllium mock-up FW components by plasma spray deposition on macro-roughened substrates. Experimental parameters, high heat flux testing and characterization results from the components are presented. No separation of the coating from the substrate was observed. Results of high heat flux testing under electron beam irradiation show performance exceeding that required for ITER FW components. Differences in macro-roughening features result in changes in the threshold absorbed heat flux before damage to the coatings occurs.**

**Keywords** beryllium, fusion reactor, low pressure plasma spray, substrate interaction, thermal properties

## 1. Introduction

The International Thermonuclear Experimental Reactor (ITER) is the next large test bed for magnetic confinement nuclear fusion energy technology. The primary nuclear fusion reaction of interest is between deuterium and tritium isotopes of hydrogen. When one deuterium atom fuses with one tritium atom, a 14.1 MeV neutron and a 3.5 MeV alpha particle are produced. The energy from these highly energetic particles is deposited primarily in the area of the divertor and blanket regions of the reactor. These regions serve to protect the remainder of the reactor from high heat loads.

The area of the blanket that is facing the high temperature plasma is called the first wall (FW). The design requirements for the ITER FW are found in Section 2.3 of the Technical Basis for the ITER Final Design (Ref 1). The FW heat flux absorbed in the cooling water is expected to be 0.25 MW/m$^2$ on average with a maximum of 0.5 MW/m$^2$. The pulse length for heating is approximately 400 s with a pulse repetition period of as short as 1800 s. Over the lifetime of ITER, the number of pulses could exceed 30,000. The material on the outer surface of the FW (facing the plasma) is beryllium metal. Beryllium (Be) is chosen for its low atomic number, oxygen gettering ability, and low tritium retention among other properties. The Be thickness on the FW is 10 mm and the maximum allowable surface temperature during operation is 700 °C. The total surface area of the Be FW is 680 m$^2$. The Be is attached to a water-cooled copper alloy heat sink that is bonded to a water-cooled stainless steel structure. The primary functions of the copper alloy are to extract the heat from the Be and channel eddy currents produced from magnetic field fluctuations. The stainless steel structure attaches the FW to the vacuum vessel and provides mechanical rigidity for the entire assembly.

Plasma spraying is being considered for the initial fabrication and the repair of the FW. Initial fabrication and repair of Be FW components by plasma spraying have several advantages as described in Ref 2 and 3. Plasma spraying allows the production of FW components from Be powder in one step vs. a bonded tile approach which requires hot pressing the Be powder, machining the tiles, and bonding the tiles to the heat sink to produce the FW components.

The primary technical challenge to successfully plasma spraying Be on a copper alloy heat sink for FW applications is the control of stresses that result from the spraying process and stresses that result from the thermal and mechanical loads which impinge on the component during operation in the fusion reactor. Careful consideration of the coefficient of thermal expansion (CTE) mismatch

**K.J. Hollis** and **B.D. Bartram,** Materials Science Division, Los Alamos National Laboratory, Los Alamos, NM; **M. Roedig,** Forschungszentrum Jülich GmbH Association KFA-EURATOM, 52425, Jülich, Germany; **D. Youchison** and **R. Nygren,** Sandia National Laboratory, Albuquerque, NM. Contact e-mail: kjhollis@lanl.gov

between the coating and substrate and thermal stresses, which arise during fabrication and in service is necessary to produce a coating that will survive both fabrication and deployed service. Therefore, strain tolerance and controlled stress relief are properties of critical importance for fusion reactor FW applications. In order to prevent cracking at the interface between the Be-coating and the heat sink, formation of brittle Cu/Be intermetallic compounds must be minimized. In addition, the Be must have high thermal conductivity to minimize surface temperature and thermal gradients. Achieving these goals in a cost-effective manner with minimal personnel exposure to Be is the challenge of the experiments described here.

Previous investigations showed that thick coatings (5-10 mm) of Be can be deposited onto copper alloys but edge lifting of the coating after fabrication was observed in all cases (Ref 4). As is observed in depositing other thick plasma-sprayed coatings, the shrinkage which results from the cooling of the deposited particles from their melting temperature to the substrate temperature causes tensile stress, referred to as quenching stress, in the sprayed coating (Ref 5). This tensile stress is often released by separation of the coating from the substrate near the edges of the coating. During high heat flux testing, this separation causes the interruption of conductive heat flow from the Be to the copper alloy and a subsequent increase in Be temperature until the coating melts or completely detaches, either of which would constitute failure of the component.

The use of macro-roughening of the substrate (substrate features $^1/_{10}$ to ½ the height of the coating) as a means of increasing adhesion and thermal stress tolerance of a coating in cyclic high heat flux conditions used has been successfully demonstrated in numerous applications of thick thermal-sprayed coatings (Ref 6-10). The application of substrate macro-roughening to plasma sprayed Be FW mock-ups is the topic of the work described here.

## 2. Experimental Procedure

### 2.1 Substrates

The substrate material used was precipitation strengthened Cu-0.65Cr-0.1Zr alloy (CuCrZr). The substrate size was 58 mm long by 22 mm wide by 19 mm high. The center of the substrate contained a 10 mm diameter coolant passage with coolant tubes extending from each end of the sample. A total of six substrates were macro-roughened and coated with Be. Three samples were coated to a Be thickness of 10 mm and the other three were coated to a Be thickness of 5 mm.

Prior to plasma spray coating, the CuCrZr substrates were machined to produce the desired macro-roughened pattern. Four of the substrates were machined with cubic projections. Two of the substrates with cubic projections had cube lengths and separations of 3 mm while the other two had lengths and separations of 1.5 mm. The larger cubes were coated with 10 mm of Be and the shorter

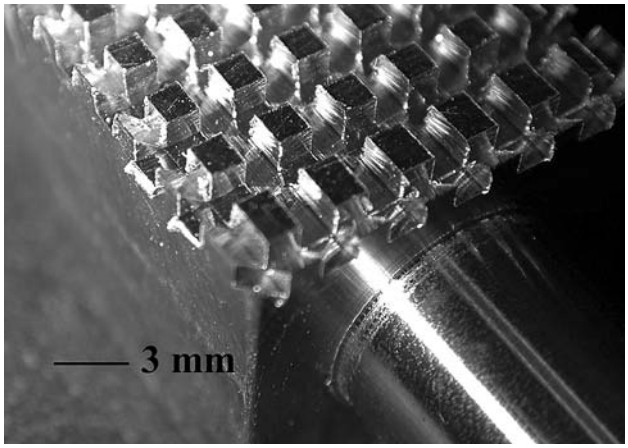


**Fig. 1** Surface pattern machined into CuCrZr alloy substrates for 5 mm thick coating

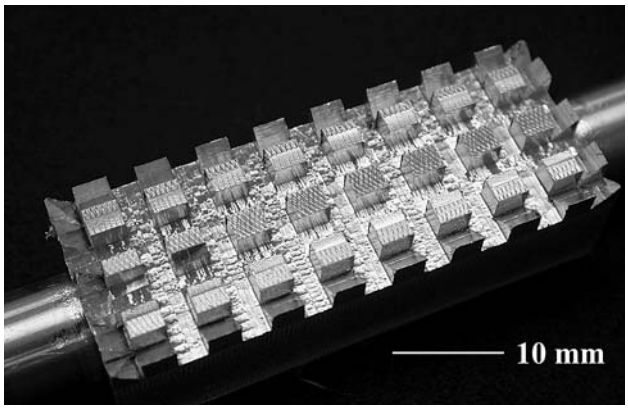


**Fig. 2** Surface pattern machined into CuCrZr alloy substrate for 10 mm thick coating

cubes were coated with 5 mm of Be. Figure 1 shows a substrate with 1.5 mm cubic projections. Slight deviations from cubic to rectangular parallelepiped dimensions as seen in the nearest row of projections in Fig. 1 were necessary at one end to cover the entire substrate. Figure 2 shows a substrate with 3 mm cubic projections. In addition to the cubic projection pattern, a dovetail projection was also used. The dovetail height was 2.3 mm with a maximum width of 4.7 mm and a sidewall angle of 75°. Coatings of 5 and 10 mm were deposited on the same dovetail patterns. Figure 3 shows a substrate with dovetail projections.

### 2.2 Beryllium Powder

Gas-atomized Be powder (product O-30 from Brush Wellman, Inc., Cleveland, OH) was used. Standard Be powder is impact attrited and is angular in shape. The gas-atomized powder was more free flowing than the attrited powder due to its spherical shape as is shown in the scanning electron microscope (SEM) image in Fig. 4. The particle size was substantially in the range of −80 +5 μm and the size distribution from sieve analysis is given in

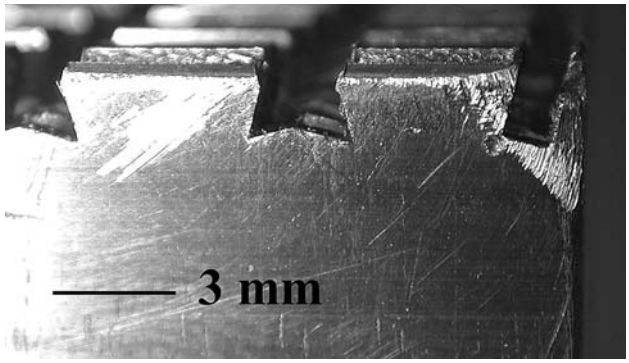


**Fig. 3** Dovetail projections machined into copper alloy substrate

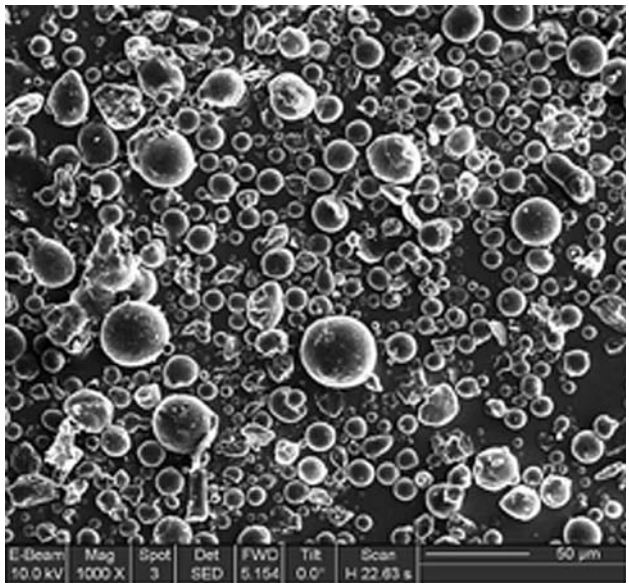


**Fig. 4** SEM image of beryllium powder used to spray mock-ups. *Note*: The powder was taken from the side wall of a container and is not an average sample of particle size

Fig. 5. The chemical composition of the powder was measured by Brush Wellman and is given in Table 1.

### 2.3 Spray Conditions

The low-pressure plasma spray (LPPS) conditions used for spraying the Be samples are given in Table 2. The torch used was a Praxair Surface Technologies, Inc. (Indianapolis, IN) SG-100 with anode model 730, cathode model 720, and gas injector model 112. The sample was cleaned and preheated using negative transferred arc (NTA) treatment prior to depositing Be. NTA was also used during deposition. Argon gas was used to cool the substrate to maintain the substrate temperature in the 600-650 °C temperature range. The maximum temperature of 650 °C was chosen to avoid over-aging the precipitation strengthened CuCrZr alloy. Thermocouples were imbedded in the substrate to monitor temperature during deposition.

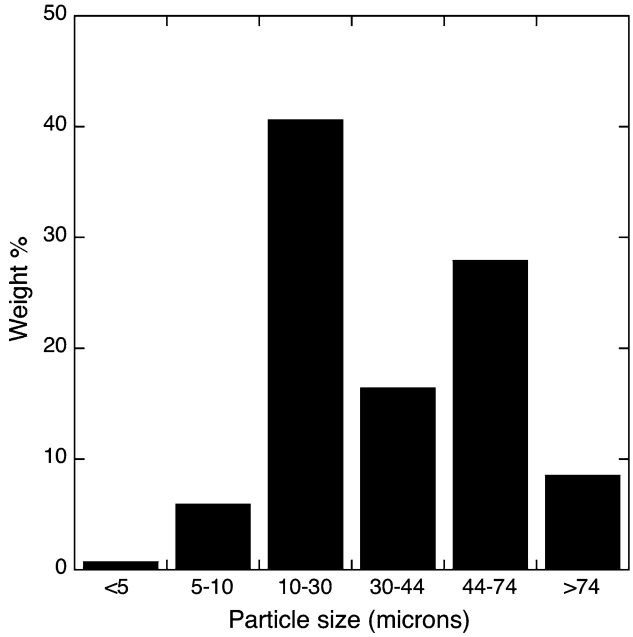


**Fig. 5** Beryllium powder size distribution

**Table 1 Beryllium powder chemical composition**

| Be | BeO | C | Fe | Al | Si |
|---|---|---|---|---|---|
| Bal | 0.64 wt.% | 0.086 wt.% | 1090 ppm | 425 ppm | 325 ppm |

**Table 2 Spray conditions for beryllium deposition**

| Spray parameter | Value |
|---|---|
| Torch current | 550 A |
| Torch arc gas | 50 slm Ar-4%$H_2$ |
| Powder gas | 2.5 slm Ar |
| Standoff distance | 95 mm |
| Substrate temp. | 600-650 °C |
| Torch speed | 10 mm/s |
| Chamber pressure | 763 hPa |

### 2.4 Coating Analysis

After spraying, the thickness of deposited Be was measured at various locations with a caliper. One sample was sectioned, polished, and examined under an optical microscope and in an SEM. Coating porosity was determined from computerized image analysis of several optical microscope images using NIH Image (Ref 11). SEM images taken in electron back-scatter mode to highlight atomic number differences were used to search for the presence of Be/Cu intermetallic compounds at the coating/substrate interface.

### 2.5 High Heat Flux Testing

The four samples with cubic projections were tested in the Jülich Divertor Test Equipment in Hot Cells (JUDITH) electron beam facility at Forschungszentrum,

Jülich, Germany. Details of JUDITH are found in Ref 12. The 5 mm thick samples were heated for 10 s then cooled for 10 s while the 10 mm thick samples were heated for 15 s and cooled for 15 s per cycle. The samples were cooled with water at 20 °C flowing 1.0 L/s. The absorbed heat flux and number of cycles were chosen to be similar to those present in ITER. The absorbed heat flux was increased until the sample under test showed a surface temperature of 800 °C.

The two samples with dovetail projections were tested at the Plasma Materials Test Facility at Sandia National Laboratories in Albuquerque, New Mexico, using the 30 kW Electron Beam Test System (EBTS). Details of the facility are given in Ref. 13. The samples were heated for 10 s and cooled for 15 s per cycle. The samples were cooled with water at 8-20 °C flowing 0.79 L/s. Like the testing at JUDITH, the absorbed heat flux and number of cycles were chosen to be similar to those present in ITER. The absorbed heat flux was increased until the sample under test showed a surface temperature of 800 °C or sample damage was observed.

## 3. Results

### 3.1 Optical Microscope Imaging

The microstructure of the Be-sprayed coating and the Be/Cu interface was examined by optical microscopy and SEM. The particular sample examined by optical microscopy and SEM was sprayed under the same conditions as the 5 mm Be-coated parts with cubic macro-roughened substrates (samples 5-1 and 5-2) delivered to JUDITH for high heat flux testing. Figure 6 shows a view of the Be-coating cross section. The image in Fig. 6, along with images of five other areas in the coating away from macro-roughening features, were separated into pore and solid material areas (thresholding operation) using computerized image analysis techniques to identify the porosity present. The area percentage of porosity was calculated by the program. The porosity, as determined by this image analysis technique, ranged from 1 to 3% by area. In addition, the areas around the substrate macro-roughening features had regions of much higher porosity. This can be seen in Fig. 7 as the dark porous area around the square substrate projection. For comparison, previous studies have found porosity in plasma sprayed Be coatings on flat substrates to be between 2 and 12% (Ref 14, 15). This level of porosity is similar to that found in the present study when considering together both areas near and away from macro-roughening features.

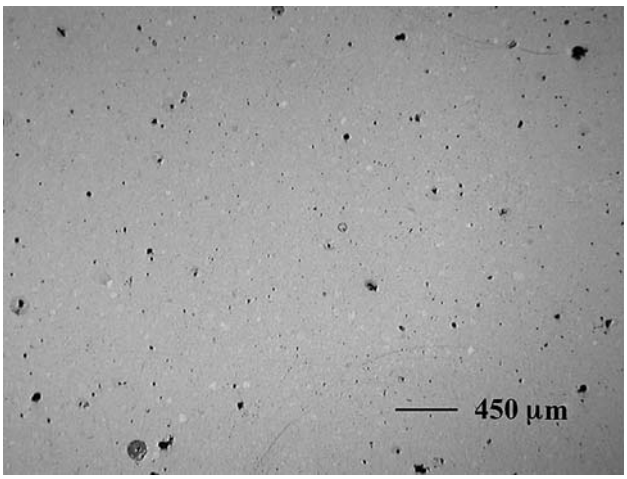


**Fig. 6** Optical microscopy image of the cross section of a 5 mm thick Be-coating sprayed onto copper

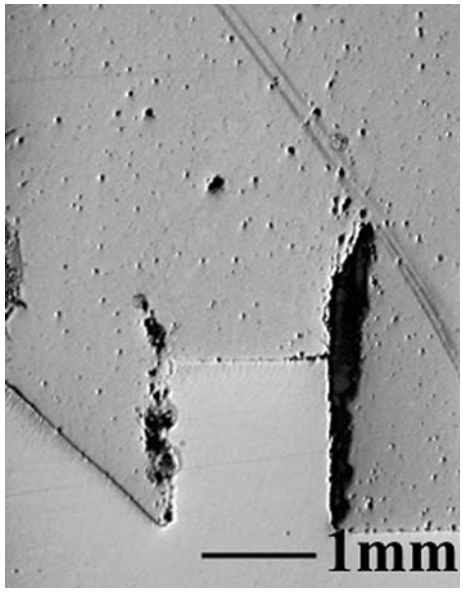


**Fig. 7** Optical microscopy image of the coating and substrate near a macro-roughening feature

### 3.2 SEM Imaging

Images of the interface between the Be-coating and the copper substrate were examined in an SEM using backscattered electron imaging. Beryllium readily reacts with copper to form brittle intermetallic compounds that can reduce ductility and toughness of the joint to unacceptable levels (Ref 16). Therefore, determining if the LPPS deposition of Be onto copper causes the formation of intermetallic compounds is important. Figure 8 shows the Be/Cu interface. The image contrast shows a dark phase material (Be) and a light phase material (Cu). There is no evidence of a third intermetallic phase with brightness between the Be and copper at the interface. Higher magnification images also failed to identify any intermetallic phase present.

### 3.3 High Heat Flux Testing

**3.3.1 JUDITH testing.** Figure 9 shows a sample with 3 mm cubic projections machined into the substrate, plasma spray coated with 10 mm of Be, and sides machined flat to remove overspray material. Two of these

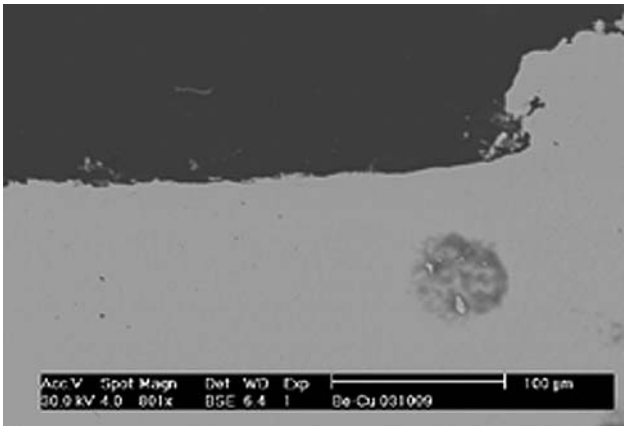


**Fig. 8** SEM back-scattered electron image of the Be (dark)/Cu (light) interface showing the absence of intermetallic compounds

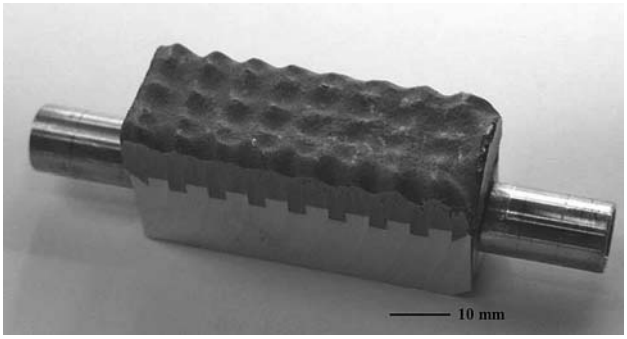


**Fig. 9** Sample with 3 mm cubic projections machined into the Cu alloy substrate and plasma sprayed with 10 mm of beryllium

nominally identical 10 mm Be-coated samples (sample number 10-1 and 10-2) were tested at the JUDITH facility. In addition, two samples (5-1 and 5-2) with 1.5 mm cubic projections machined into the substrate and 5 mm thick Be-coatings were also tested. Unlike plasma-sprayed Be samples in previous studies (Ref 4) there was no indication of coating separation from the substrate near the edges of the samples.

The test schedules for samples 5-1, 5-2, 5-3, 10-1, 10-2, and 10-3 are shown in Table 3. The incident heat flux is the total electron beam output incident on the sample, and the absorbed heat flux is measured from calorimetry of the sample cooling water. Testing generally started at the lowest heat flux listed and increased to the highest heat flux.

Sample 5-1 was tested for 100 cycles at 2.0 MW/m$^2$ with no increase in surface temperature. Damage on the ends of the sample occurred after 320 cycles at 3.0 MW/m$^2$ absorbed heat flux. However, the center of the sample remained largely undamaged and the testing continued. Surface temperature at the center of the sample heated surface was measured by infrared pyrometry and is shown for samples 5-1, 5-2, and 5-3 as a function of heat flux in Fig. 10. The surface temperature for sample 5-1 at the start (cycle 1) of 3.0 MW/m$^2$ testing is lower than the

**Table 3 Incident and absorbed heat flux and thermal cycles for the Be samples**

| Sample | Incident heat flux, MW/m$^2$ | Absorbed heat flux, MW/m$^2$ | % Absorbed | Cycles |
|---|---|---|---|---|
| 5-1 | 2.4 | 2.0 | 83 | 100 |
| 5-1 | 3.36 | 3.0 | 89 | 1000 |
| 5-1 | 4.0 | 3.5 | 88 | 6 |
| 5-2 | 2.4 | 2.0 | 83 | 100 |
| 5-2 | 3.36 | 3.0 | 89 | 1000 |
| 5-2 | 4.42 | 4.05 | 92 | 100 |
| 5-3 | 1.3 | 1.0 | 77 | 1000 |
| 5-3 | 2.5 | 1.72 | 69 | 1 |
| 5-3 | 2.9 | 2.1 | 72 | 1 |
| 5-3 | 3.4 | 2.5 | 73 | 1 |
| 5-3 | 3.47 | 2.45 | 70 | 1 |
| 5-3 | 3.1 | 2.0 | 65 | 410 |
| 10-1 | 1.83 | 1.5 | 82 | 1000 |
| 10-1 | 2.5 | 2.0 | 80 | 100 |
| 10-1 | 2.6 | 2.25 | 87 | 1 |
| 10-2 | 1.83 | 1.55 | 85 | 1000 |
| 10-2 | 2.35 | 2.05 | 87 | 100 |
| 10-2 | 2.88 | 2.5 | 87 | 50 |
| 10-3 | 0.95 | 0.6 | 64 | 1 |
| 10-3 | 1.22 | 0.81 | 66 | 1 |
| 10-3 | 1.57 | 0.99 | 63 | 1 |
| 10-3 | 1.78 | 1.15 | 64 | 1 |
| 10-3 | 1.45 | 1.0 | 69 | 856 |

temperature at the end (cycle 1000) by 30 °C indicating a slight decrease in heat conduction through the sample during the testing. The absorbed heat flux was increased to 3.5 MW/m$^2$ for six cycles during which time the damage on the ends of the samples worsened ending the test.

Sample 5-2 was tested for 100 cycles at 2.0 MW/m$^2$ with no increase in surface temperature. After 1000 cycles at 3.0 MW/m$^2$ there was only a slight (30 °C) increase in

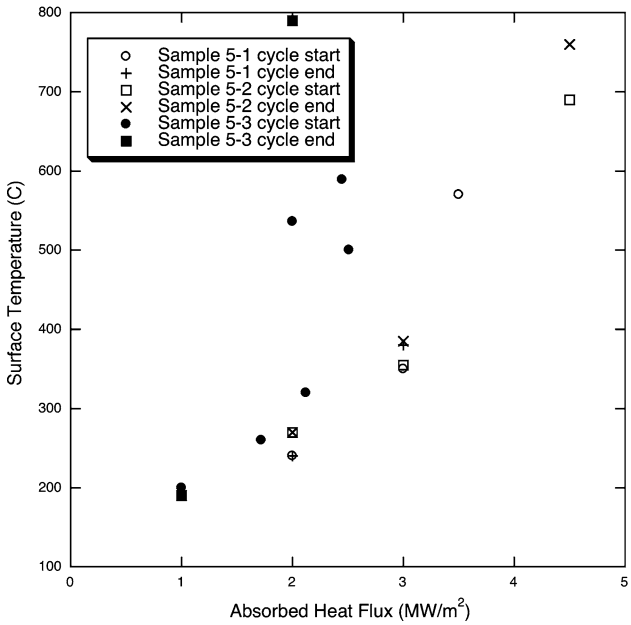


**Fig. 10** Surface temperature and cooling water absorbed heat flux for samples 5-1, 5-2 and 5-3

surface temperature. Damage on one end of the sample occurred during a screening cycle at 3.4 MW/m$^2$ absorbed heat flux. Testing continued up to 4.05 MW/m$^2$ absorbed heat flux for 100 cycles but with continuously increasing surface temperature.

Sample 10-1 was tested for 1000 cycles at 1.5 MW/m$^2$ with only a slight increase (16 °C) in surface temperature. The absorbed heat flux was increased to 2.0 MW/m$^2$ for 100 cycles during which the surface temperature increased 13 °C. Damage on one end of the sample occurred during cycling at 2.0 MW/m$^2$ absorbed heat flux. Testing continued up to 2.25 MW/m$^2$ absorbed heat flux for one screening cycle. Surface temperatures and absorbed heat flux values for samples 10-1, 10-2, and 10-3 are shown in Fig. 11.

Sample 10-2 was tested for 1000 cycles at 1.55 MW/m$^2$ with only a slight increase (10 °C) in surface temperature. The absorbed heat flux was increased to 2.05 MW/m$^2$ for 100 cycles during which the surface temperature increased 8°C. Damage on the sample occurred during cycling at 2.5 MW/m$^2$ absorbed heat flux. A gradual increase in surface temperature during cycling at 2.5 MW/m$^2$ was observed with a temperature of 685 °C at cycle 1 and a temperature of 750 °C at cycle 50.

**3.3.2 EBTS Testing.** Two samples were tested at the EBTS facility. Sample 5-3 used the dovetail macro-roughening pattern shown in Fig. 3 and was coated with 5 mm of Be. A second sample (10-3) with the same substrate design was coated with 10 mm of Be. Like the samples tested at JUDITH, there was no indication of coating separation from the substrate near the edges of the samples after fabrication.

Sample 5-3 was tested for 1000 cycles at 1.0 MW/m$^2$ with no increase in surface temperature. The surface temperature at the end of the 1000 cycles was slightly lower than the start temperature due to a correction in the emissivity of the pyrometer. Thermocouple data in the substrate indicated no difference in temperature from the start to the end of the 1000 thermal cycles so the surface temperature likely changed little during cycling. Next, screening cycles at several power levels were performed. The surface temperature from 1.72, 2.1, 2.5, and 2.45 MW/m$^2$ are shown in Fig. 10. The surface temperature increased gradually between the cycles at 1.72 and 2.12 MW/m$^2$. However, damage occurred during the screening shot at 2.5 MW/m$^2$. This is shown in Fig. 10 as the large increase in surface temperature between the screening shots at 2.1 (320 °C) and 2.5 MW/m$^2$ (500 °C). Further damage occurred during the subsequent screening cycle at 2.45 MW/m$^2$ (589 °C) as indicated by the increase in surface temperature. After the screening shots, testing continued at 2.0 MW/m$^2$ absorbed heat flux with a starting surface temperature of 536 °C and a gradual increase in temperature to 790 °C. The testing was halted after 410 cycles due to increasing sample damage as indicated by the high surface temperature.

Damage occurred in sample 10-3 during a screening cycle at 1.15 MW/m$^2$ absorbed heat flux before thermal cycling began. The damage can be deduced from the variation in surface temperature of the cycle at 1.15 MW/m$^2$ (350 °C) from the linear trend in surface temperature vs. absorbed heat flux observed in the cycles at 0.6 (184 °C), 0.81 (225 °C), and 0.99 MW/m$^2$ (274 °C) as seen in Fig. 11. Further damage occurred during screening cycles resulting in a surface temperature of 350 °C for the start of thermal cycling at 1.0 MW/m$^2$ absorbed heat flux. After starting at 350 °C, the surface temperature increased gradually to 550 °C where it remained for the duration of the testing. The testing was halted after 856 cycles due to the detachment of a small surface area at the end of the sample. However, the surface temperature was not increasing with additional cycles when the test was halted.

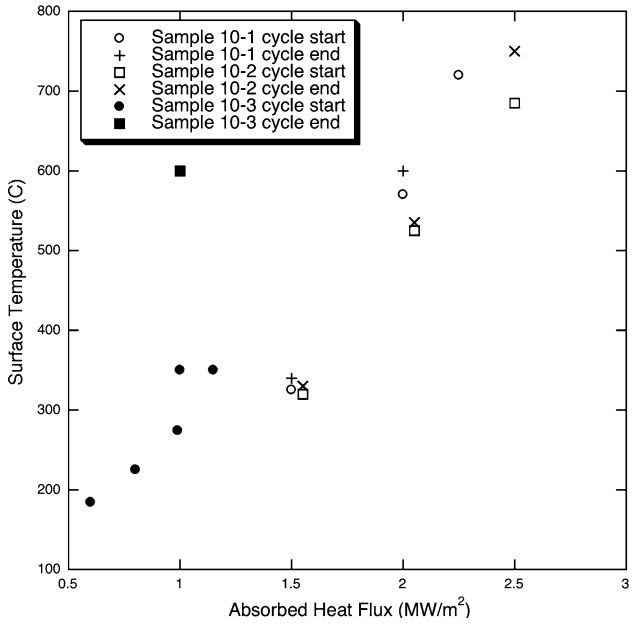


**Fig. 11** Surface temperature and cooling water absorbed heat flux for samples 10-1, 10-2 and 10-3

## 4. Discussion

### *4.1 Relative Thermal Conductivity*

Using the data collected during high heat flux testing, a comparison of Be thermal conductivity was performed. From the data points in Fig. 10 and 11, the relative thermal conductivity of the coatings can be compared using the surface temperature for a given absorbed heat flux. If only the data points before coating damage has occurred are considered, a comparison of relative thermal conductivity between the samples with dovetail features and cubic features is possible. For example, in Fig. 10, the data points for sample 5-3 with surface temperature below 400 °C were recorded before coating damage. These data points show an approximately linear variation in surface temperature with absorbed heat flux as would be expected before radiation heat losses become significant. Likewise, the data points for samples

5-1 and 5-2 below a surface temperature of 400 °C were recorded before coating damage occurred. A comparison of the surface temperatures (below 400 °C) as a function of absorbed heat flux for samples 5-1, 5-2, and 5-3 show similar values. However, exact comparison between the JUDITH and EBTS surface temperatures is not possible since the temperatures were measured in slightly different ways. Therefore, it is possible to conclude only that the surface temperatures for a given heat flux (and by implication the thermal conductivities of the coatings) were similar for all samples. The spray conditions for all samples were the same except for the substrate macro-roughening pattern and the coating thickness. This indicates that the different macro-roughening patterns did not result in significantly different thermal conductivity values of the coatings.

### 4.2 Damage Threshold

Significant differences were discovered in the damage threshold of the various samples. Damage in sample 5-3 first occurred at an absorbed heat flux of 2.5 MW/m$^2$. By contrast, sample 5-1 was not damaged until 3.0 MW/m$^2$ and sample 5-2 was not damaged until 3.4 MW/m$^2$. The 10 mm thick coatings showed a similar trend with damage in sample 10-3 occurring at 1.15 MW/m$^2$ while sample 10-1 was not damaged until 2.0 MW/m$^2$ and sample 10-2 was not damaged until 2.5 MW/m$^2$. These trends indicate that the samples with dovetail macro-roughening were damaged at lower absorbed heat flux levels than similar samples with cubic macro-roughening.

## 5. Conclusions

In this study, the use of large (23-46% of coating thickness) cubic and dovetail substrate projections has been shown to prevent edge lifting of 5 and 10 mm thick Be coatings during fabrication by plasma spraying and testing under ITER first wall relevant conditions. In addition, the coatings have low porosity (1-3%) away from the macro-roughening features, and appear to avoid beryllium/copper intermetallic formation at the coating/substrate interface.

All samples in this study exceeded the ITER required average heat flux of 0.25 MW/m$^2$ and maximum heat flux of 0.5 MW/m$^2$ before damage was detected. Damage in the 10 mm thick Be-coating samples occurred at 4.6 (sample 10-3), 8 (sample 10-1), and 10 (sample 10-2) times the average expected heat flux of 0.25 MW/m$^2$. For the 5 mm thick Be-coating samples, damage occurred at 10 (sample 5-3), 12 (sample 5-1), and 13.6 times the average expected heat flux. The samples had similar thermal conductivity values based on a comparison of surface temperatures at a given absorbed heat flux for the 5 mm thick coating samples. Despite the similar thermal conductivity, the absorbed heat flux where damage occurred was higher for the cubic macro-roughened samples than for the dovetail macro-roughened samples. Further analysis of the mode of thermal damage through destructive examination of the samples to determine crack propagation characteristics is necessary to better understand the differences in strain relief observed. Such work is anticipated in future studies.

## Acknowledgments

The authors gratefully acknowledge the assistance from Sam Atencio, Terri Abeln, and Joann Herrera with metallographic preparation, Maria Peters with SEM analysis, and Beverly Aikin with plasma spraying of the samples. Project direction and funding from Mario Merola of the European Fusion Development Agreement are also gratefully acknowledged.

## References

1. ''Technical Basis for ITER Final Design'', G A0 FDR 1 01-07-13 R1.0, International Atomic Energy Agency, Vienna, Austria. Also available at www.ITER.org
2. M.F. Smith, R.D. Watson, R.T. McGrath, C.D. Croessman, J.B. Whitley, and R.A. Causey, Concept for a Beryllium Divertor with In-Situ Plasma Spray Surface Regeneration, *J. Nucl. Mater.*, 1990, **171**, p 158-164
3. R.G. Castro, P.W. Stanek, and K.E. Elliott, The Structure, Properties and Performance of Plasma-sprayed Beryllium for Fusion Applications, *Phys. Scr.*, 1996, **T64**, p 77-83
4. R.G. Castro, K.E. Elliott, R.D. Watson, D.L. Youchison, and K.T. Slattery, Fabrication and High Heat Flux Testing of Plasma Sprayed Beryllium ITER First Wall Mock-ups, *J. Nucl. Mater.*, 1998, **258-263**, p 252-257
5. S. Kuroda and T.W. Clyne, The Quenching Stress in Thermally Sprayed Coatings, *Thin Solid Films*, 1991, **200**, p 49-66
6. H.S. Ingham and A.P. Shepard, Flame Spray Handbook1Metco Inc, New York, 1964, p A9-A32
7. D.H. James, A Review of Experimental Findings in Surface Preparation for Thermal Spraying, *J. Mech. Work. Technol.*, 1984, **10**, p 221-232
8. F. Bordeaux, R.G. Saint Jacques, C. Moreau, S. Dallaire, and J. Lu, Thermal Shock Resistance of TiC Coatings Plasma Sprayed onto Macroroughened Substrates, *Surf. Coat. Technol.*, 1992, **53**, p 49-56
9. W. Mallener, Tungsten Coatings for Divertor Wings, *Thermal Spray 2001: New Surfaces for a New Millennium*, C.C. Berndt, K.A. Khor, and E.F. Lugscheider, Eds., May 28-30, 2001 (Singapore), ASM International, 2001, p 55-60
10. J.L. Smialek, Improved Oxidation Life of Segmented Plasma Sprayed 8YSZ Thermal Barrier Coatings, *Thermal Spray 2003: Advancing the Science & Applying the Technology*, Vol. 2, B.R. Marple and C. Moreau, Eds., May 5-8, 2003 (Orlando, FL), ASM International, 2003, p 1463-1470
11. Public domain NIH Image program developed at the U.S. National Institutes of Health, http://rsb.info.nih.gov/nih-image/
12. R. Duwe, W. Kühnlein, and H. Münstermann, The New Electron Beam Facility for Materials Testing in Hot Cells-Design and Preliminary Experience, *Fusion Technology 1994, Proceedings of the 18th Symposium on Fusion Technology (SOFT)*, Vol. 1, K. Herschbach, W. Maurer, and J.E. Vetter, Eds., Aug 22-26, 1994 (Karlsruhe, Germany), Elsevier, 1995, p 355-358
13. D.L. Youchison, J.M. McDonald, and L.S. Wold, High Heat Flux Testing Capabilities at Sandia National Laboratories, New Mexico, HTD-vol. 301, *Heat Transfer in High Heat Flux Systems*, A.M. Khounsary, Ed., ASME Book No. G00956, 1994
14. R.G. Castro, A.H. Bartlett, K.J. Hollis, and R.D. Field, The Effect of Substrate Temperature on the Thermal Diffusivity and

Bonding Characteristics of Plasma Sprayed Beryllium, *Fusion Eng. Des.*, 1997, **37**, p 243-252
15. R.A. Anderl, R.J. Pawelko, G.R. Smolik, and R.G. Castro, "Steam Chemical Reactivity of Plasma-Sprayed Beryllium", Idaho National Engineering and Environmental Laboratory Report INEEL/CON-98-00019, 1998
16. C.H Cadden, W.D. Bonivert, B.C. Odegard, and R.D. Watson, Beryllium-Copper Joining Techniques for Use on Plasma-Facing Components, *SOFE ,95: Seeking a New Energy Era: Symposium on Fusion Engineering*, G.H. Miley and C. Elliott, Eds., Sept. 30-Oct 5, 1995 (Champaign, IL), IEEE, 1996, p 377-380